OPEN ACCESS

UNIVERSITY OF THE
WEST *of* SCOTLAND
UWS

UWS Academic Portal

Detection, biophysical effects, and toxicity of polystyrene nanoparticles to the cnidarian Hydra attenuata

Auclair, Joëlle; Quinn, Brian; Peyrot, Caroline; Wilkinson, Kevin James; Gagné, François

Link to publication on the UWS Academic Portal

Auclair, J., Quinn, B., Peyrot, C., Wilkinson, K. J., & Gagné, F. (2020). Detection, biophysical effects, and toxicity of polystyrene nanoparticles to the cnidarian Hydra attenuata. Environmental Science and Pollution Research.

1 Detection, biophysical effects and toxicity of polystyrene nanoparticles to the
2 cnidarian *Hydra attenuata*

3 Joëlle Auclair, Brian Quinn, Caroline Peyrot, Kevin JamesWilkinson, François Gagné*

4 1. Aquatic Contaminants Research Division, Environment and Climate Change Canada, 105
5 McGill, Montréal, Québec, Canada H2Y 2E7. Francois.gagne@canada.ca 2. School of Health and
6 Life Sciences, University of the West of Scotland, Paisley, Scotland, United Kingdom PA1 2BE.
7 3. Chemistry Department, Montreal University, Montréal, Québec, Canada H2V 2B8.

8 * Corresponding author: François Gagné: francois.gagne@canada.ca

Abstract

10 The occurrence of nanoplastic particles (NPs) in the environment has raised concerns about the
11 ecotoxicological risk to aquatic ecosystems. The purpose of this study was to examine the
12 bioavailability and toxicity of 50 and 100 nm transparent polystyrene NPs to the cnidarian *Hydra*
13 *attenuata*. The hydra were exposed to increasing concentrations of 50 and 100 nm NPs (1.25, 2.5,
14 5, 10, 20, 40 and 80 mg/L) for 96 h at 20°C followed by a 24h-depuration step. Hydra were
15 analysed for morphological changes, bioaccumulation of NPs using a novel assay for polystyrene
16 NPs, oxidative stress (lipid peroxidation), polar lipids, lipid-like liquid crystals (LCs) and viscosity
17 changes in the post-mitochondrial fraction. The results revealed that the organisms accumulated
18 detectable amounts of NP in a concentration dependent manner for both the 50 and 100 nm NP
19 that persisted after 24 h in clean media. Changes in morphology were observed with a 50% effect
20 concentration of 3.6 and 18 mg/L for the 50 and 100 nm diameter NPs respectively. However
21 based on the particle density, the 100 nm proved to be 1.7 times more toxic than the 50 nm NPs.
22 Exposure to NPs led to decreased biomass, lipid peroxidation (LPO), increased polar lipids levels,
23 viscosity and formation of LCs at the intracellular level. In the more toxic NP (100 nm), NPs in
24 tissues were correlated with LCs, polar lipids and LPO levels. It appears that the formation of
25 organized LCs and polar lipids of NPs in cells was involved with NPs toxicity and could represent
26 a yet unidentified, detoxifying/bioactivation mechanism against colloidal plastics in cells. In
27 conclusion, NPs are bioavailable to hydra and lead to LPO and lipid mobilisation in hydra. The
28 capacity of increasing lipid mobilization and LCs could determine the size-dependence toxicity of
29 NPs.

30 Key words: nanoplastics, polystyrene, hydra, oxidative stress, neutral lipids.

Introduction

32 Plastic products are ubiquitous in the environment as they permeate many aspects of our daily

33 lives. They can be found in various products such as coatings, cosmetics, wiring, packaging, film

34 covers, bags and miscellaneous containers (Al-Salem et al., 2009). Although many plastics are

35 recycled, they are unfortunately still found in most water bodies including rivers and oceans

36   persisting for decades in the environment. Plastic particles could degrade in the environment from

37   abiotic (physical abrasion) and biotic factors leading to microplastics (operationally defined as

38   materials between 1 µm to 5 mm) and nanoplastics (NPs; 1 to 100 nm) (Lambert and Wagner,

39   2016). The long-term degradation of plastic materials will lead to staggering quantities of NPs in

40   the environment. Polystyrene-based plastics are one of the most abundant forms of plastics

41   representing circa 10% of total plastic production (Verschcoor et al., 2017) and can remain in the

42   environment for hundreds of years (Ho et al., 2018). Although microplastic materials can clog and

43   damage the digestive system and skin in birds and aquatic animals, the small size of NPs makes

44   them permeable to tissues and cells whereas they can accumulate and produce unknown effects at

45   the intracellular/macromolecular levels. Indeed, internalized NPs were shown to damage cells by

46   apoptosis, protein denaturation/fibrillation and the formation of organized lipophilic liquid crystals

47   (LCs) in cells (Colvin and Kulinowski, 2007; Wang et al., 2013; Gagné et al., 2019a). Although

48   several studies can be found on the effects of NPs in marine organisms, there are a limited number

49   of studies on the toxicity of NPs in freshwater invertebrates.

50   The freshwater hydranth *Hydra attenuata* is commonly found in freshwater ecosystems and is a

51   well-recognized test organisms in aquatic toxicity studies (Blaise and Kusui, 1997; Pascoe et al.,

52   2003; Quinn et al., 2012). The hydra is a simple organism composed of a tube-like structure, with

53   a foot attaching to a solid substrate and a head composed of 4-6 long tentacles for food capture.

54   The toxic intensity (reversible sub-lethal to irreversible lethal effects) can be conveniently

55   observed trough a stereomicroscope by a series of morphological changes such as antennae

56   shortening, loss of antennae and compressed tube. More recently, the hydra was used to examine

57   the toxicity of both microplastics (Murphy and Quinn, 2018) and nanoplastics (Gagné et al,

58   2019b). Hydra were able to ingest small microplastics fragments from face wash soaps that

59 compromised feeding activity and displayed sub-lethal stress by regression of antenna. These

60 studies revealed that microplastics could reduce feeding activity whereas NPs could significantly

61 induce reversible morphological changes and increase polar lipids levels in hydra. In the case of

62 polystyrene NPs, the styrene-based surface provides a hydrophobic environment (aryl benzene)

63 which could induce strong hydrophobic interactions given the high surface area of nanoparticles.

64 It is hypothesized that the introduction of the hydrophobic surface of NPs could elicit changes on

65 lipid mobilization and other macromolecules such as less polar proteins/peptides at the surface of

66 the NPs.

67 The purpose of this study was therefore to examine the bioavailability and toxicity of 50 and 100

68 nm polystyrene NPs in *Hydra attenuata*. The bioavailability of NPs was determined by a novel

69 fluorescent probe methodology. Toxicity effects were determined by both morphological changes

70 and sublethal biomarkers. The latter consisted in changes in lipid peroxidation, polar lipid levels,

71 microviscosity changes and the formation of anisotropic LCs. The mode of action based on

72 hydrophobic interactions of NPs was examined in hydra exposed to NPs.

73
74 Materials and Methods
75
76 ***Preparation and exposure of NPs to hydra***

77 Transparent, unlabeled polystyrene nanoplastics (NP) of 50 and 100 nm diameter were obtained

78 from Polyscience Inc (USA). The hydra were maintained in a media consisting of 1 mM $CaCl_2$

79 and 0.5 mM TES (N-tris [hydroxymethyl]methyl 1-2- aminoethanesulfonic acid), pH 7.0 at 20ºC

80 as previously described (Blaise and Kusui, 1997) and were fed each day with preparations of live

81 *Artemia salina* brine shrimps. Exposure tests were conducted in 12-well microplates with three

82 animals placed in each well (n=9 hydra per treatment) containing 4 mL of media. The NP

83 suspension was prepared at 0.5 g/L in MilliQ water to prevent aggregation, with the final dilutions

84   prepared in hydra media. The size distribution of these NPs were examined in MilliQ water and in

85   the incubation media using dynamic light scatter instrument with an operating laser at 532 nm

86   (Mobius Instrument, Wyatt Technologies, Santa Barbara, CA, USA). Unexposed hydra

87   maintained in culture media only served as controls. The exposure concentrations used were 0,

88   1.25, 2.5, 5, 10, 20, 40 and 80 mg/L corresponding to 0.32, 0.64, 1.29, 2.57, 5.15, 1.03, 2.06×10^{12}

89   nanoparticles/L for the 50 nm NP and 0.04, 0.079, 0.159, 0.318, 0.636, 1.27, and 2.54×10^{11}

90   nanoparticles/L for 100 nm NP respectively. Hence, on a mass basis, 50 nm NP contains 8 times

91   more particles than the 100 nm NP. The selected concentration were chosen to attain a lethal

92   concentration which was in ppm range. These concentrations are not necessarily environmentally

93   realistic but could be attained in a spillage situation (e.g. sediments contaminated by miscellaneous

94   plastics compounds released by a nearby industry or source).

95   After the exposure period (96 h), changes in hydra morphology were determined under a 6 x

96   stereomicroscope based on the Wilby scale (Wilby, 1989). Normal control animals maintained a

97   normal size with long and slender tentacles; sub-lethal (reversible) effects consisting of hydra

98   showing clubbed or reduced tentacles length and lethal (irreversible) effects consisting in shrunken

99   hydra at the tulip or disintegrated stages. Representative examples for each morphological changes

100   are presented in Figure 1. The number of hydra with morphological changes was the variable used

101   to estimate the 50 % effects concentration (EC50) and the 50% lethal concentration (LC50). The

102   positive control consisted of $ZnSO_4$ (LC50 of 1 mg/L; 0.7-1.3 mg/L 95% confidence interval)

103   which was used for quality assurance control. A subset of hydra at the low exposure group and

104   controls (0, 1.25, 2.5 and 5 mg/L) were allowed to depurate in clean media for 24 h before freezing

105   to determine the elimination potential of the NPs and persistence of toxicity. At the end of the

106   morphological assessment, the hydra media was removed from the wells, the hydra washed in 1

107   mL of media, detached and suspended in 250 µL homogenisation buffer consisting of 50 mM NaCl

108   containing 10 mM Hepes-NaOH, pH 7.4, 0.1 mM dithiothreitol and 0.1 µg/mL apoprotinin

109   (protease inhibitor). Samples were stored at -85°C for NP uptake and biomarker analyses. The

110   hydra were homogenized using an hand-held pestle tissue grinder (Canlab, ON, Canada). The

111   homogenate was allowed to settle on ice for 30 min. Total protein contents in the homogenate were

112   determined using the Coomassie Brillant Blue methodology in clear 96-well microplates

113   (Bradford, 1976). Serum bovine albumin was used for calibration.

114   *Detection of NPs in hydra*

115   Detection of polystyrene NPs was performed using the molecular rotor probe methodology

116   (Gagné, 2019). The probe consisted of a 10 mM stock solution of 9-(dicyanovinyl)-julolidine

117   (DCVJ) in ethanol, diluted to 10 µM in MilliQ water on the day of analysis. For the assay, 20 µL

118   of the homogenate was mixed with 180 µL of 10 µM of DCVJ probe in 96-well dark microplate.

119   Fluorescence was measured at 620 nm and 520 nm emission at 450 nm excitation for NP and

120   viscosity measurements respectively. Standard solutions of polystyrene NPs at 50 nm diameter

121   (0.05 and 0.1 µg/mL) were prepared for instrument calibration where 1 RFU corresponds to 1

122   µg/mL NP. The data weas expressed a relative fluorescent units-RFU /mg proteins.

123   *Early biological effects of NPs*

124   The viscosity of the homogenate was determined by the DCVJ probe at the reported emission

125   wavelength (520 nm emission; 450 nm excitation) for viscosity assessment (Haidekker et al.,

126   2001). The viscosity of a media could be defined as the resistance of molecules to movement in

127   space at a given temperature. The DCVJ is a molecular rotor probe where energy is dispersed by

128   either by kinetic rotation or by fluorescence. As the viscosity increases, rotation is limited and

129   fluorescence increases to compensate this restriction. A volume of 20 µL of the homogenate was

130   mixed with 180 µL of DCVJ probe as described above. Standard solutions of glycerol were used

131   for calibration for instrument calibration where 1 RFU corresponds to 10 µg/mL of glycerol. The

132   formation of dissipative structures such as liquid crystals (LCs) in the homogenate was determined

133   using fluorescence polarisation spectroscopy (Gagné et al., 2019a). The hydrophobic fluorescent

134   octadecyl ester (FOE) probe was used to detect the formation of LCs in hydra exposed to NPs. The

135   FOE probe was dissolved in dimethylsulfoxide at 1 mM concentration and kept at room

136   temperature in the dark. On the day of analysis, the FOE probe was diluted at 10 µM in 10 mM

137   KH_2PO_4 and Hepes-NaOH, pH 7.4, containing 140 mM NaCl. A 20 µL volume of the homogenate

138   was mixed with 200 µL of 10 µM FOE and fluorescence polarization was determined at 485 nm

139   excitation and 520 nm emission. Fluorescence polarisation was calculated by determining the ratio

140   between the perpendicular and parallel direction of the emission signal (perpendicular-parallel

141   fluorescence / perpendicular+parallel fluorescence) using dichroic mirrors (Synergy-4, Biotek

142   instrument, USA). Standard solutions of 50 nm NPs (0.05, 0.1 and 0.15 µg/mL) were prepared

143   since the polarization was shown to be concentration dependent in the presence of homogenate

144   extract (Gagné et al. 2019a). The fluorescence polarization data were imported to an Excel

145   Spreadsheet and analysed with SYSTAT software (version 13.2; USA). Fluorescence polarization

146   was measured in the same of amount of homogenate proteins (10 µg/mL).

147   Lipid peroxidation (LPO) was determined in hydra homogenates using the thiobarbituric acid

148   method (Gagné, 2014) using a miniaturized adaptation for small volumes in 384-well microplates.

149   A volume of 10 µL of the homogenate was mixed with 20 µL of 10% trichloroacetic acid

150   containing 1mM FeSO4 and 10 µL of 0.7% thiobarbituric acid in 384 wells dark microplates. The

151   mixture was placed at 75 °C for 10 min, cooled at room temperature before taking fluorescence

152 measurements. Fluorescence readings were taken at 540 nm excitation and 600 nm emission using

153 standard solutions of tetramethoxypropane (stabilized form of malonaldehyde) for calibration in

154 the blank media (homogenization buffer only). Results were expressed as µg thiobarbituric acid

155 reactants (TBARS)/mg total proteins in the homogenate.

156 The polar fraction of lipids in the homogenate was determined using the Nile red methodology

157 (Greenspan and Fowler, 1985). Nile red was prepared as 10 mM in methanol and diluted to 10 µM

158 in MilliQ water. A 20 µL volume of the homogenate was mixed with 180 µL of Nile red probe.

159 After 10 min, fluorescence was measured at 500 nm excitation and 650 nm emission (Synergy 4,

160 Biotek microplate reader, USA). Instrument calibration was achieved with standard solutions of

161 Tween-20 (0.01 to 0.05%). Data was expressed as relative fluorescence units (RFU)/mg proteins

162 in the homogenate.

163 *Data analysis*

164 The study design examines the bioavailability and toxicity in hydra exposed to the 7 increasing

165 concentrations of 50 and 100 nm NPs. The 96-h toxicity (50 % lethal concentration) was

166 determined using the Spearman-Karber method and the 96-h sub-lethal effect concentration (50%

167 effect concentration) using the Log-logit method (Finney, 1964). Data normality and homogeneity

168 of variance were verified using the Shapiro-Wilk and Bartlett tests respectively. The data was

169 analysed using analysis of variance and critical differences between the controls and exposure

170 concentrations were determined using the Least Square Difference test. The trends between the

171 data were also analyzed using Pearson-moment correlation and principal component analysis. All

172 tests were performed using the SYSTAT software (version 13). Significance was set at $p < 0.05$.

173 Results

174   On a mass basis, the stock solutions of 50 nm polystyrene NPs (6.7×10^{14} particles/mL) contained

175   8 times more particles than the 100 nm NPs (8.3×10^{13} particles/mL). The size distribution of the

176   NPs were analyzed using dynamic light scattering and revealed that the NPs were distributed at

177   the specific diameter (50 and 100 nm) and did not form aggregates. The levels of NPs was

178   determined using the DCVJ probe methodology in hydra exposed for 96h to the NPs and following

179   a 24h depuration with the low concentrations (1.25-5 mg/L) and controls (Figure 2). The analysis

180   revealed that hydra accumulated both sizes of NPs in a concentration dependent manner. For the

181   50 nm NPs, the NPs were detected at the lowest concentration (1.25 mg/L) which persisted after a

182   24h depuration period. For the 100 nm, the NPs in hydra at the lowest concentration were more

183   abundant on a mass basis than the 50 nm NPs suggesting that the 100 nm NPs were more

184   bioavailable than 50 nm NP. Indeed, hydra accumulated 24 times more NPs with the 100 nm

185   diameter size even though they were 8 times less abundant than the 50 nm NPs. Although the

186   probe was shown to react with NPs in vitro, we could not determine if a small fraction was still

187   attached on the tentacles and in the gut although the hydra were washed. This is why a 24-

188   depuration period was done to determine if the NPs in Hydra could be removed in clean media

189   (where most of the NPs were still present at that time). The toxicity of the hydra was examined

190   based on the characteristic morphological changes (Figure 1). Although no mortality was observed

191   based on the complete regression/destruction of the hydra, the EC50 based on the shortened

192   morphology of the hydra was 3.6 (9.22×10^{11} particles/mL) and 18.4 mg/L (5.81×10^{11}

193   particles/mL) for the 50 and 100 nm NPs (Table 1). Hence, despite having a higher EC50, the 100

194   nm NPs were circa 1.7 times more toxic than the 50 nm on a particle basis. The biomass of hydra

195   was also significantly reduced at 14 (3.58×10^{12} particles/mL) and 28 mg/L (8.8×10^{11}

196   particles/mL) for the 50 and 100 nm NPs respectively, showing again that the 100 nm NPs

197   produced more toxicity than the 50 nm NPs on a particle amount basis.

198   The influence of NPs on the viscosity in hydra tissues was examined (Figure 3) and found to

199   increase in hydra extracts for both NPs sizes. For the 50 nm NPs, the viscosity increased in a

200   concentration dependent manner at concentrations > 2.5 mg/L. Viscosity persisted following the

201   24h depuration period with a significant increase at 2.5 mg/L. Correlation analysis revealed that

202   viscosity was significantly correlated with biomass (r=-0.56) and NPs in tissues (r=0.60) (Table

203   2). For the 100 nm, we obtained a peculiar bell-shaped response curve with an increase in viscosity

204   at low concentrations up to 2.5 mg/L NPs followed by a decrease at the higher concentrations. The

205   increased viscosity persisted after 24h depuration period with a significant increase at 5 mg/L

206   compared to controls. The formation of lipid-like LCs was examined using fluorescence

207   polarization spectroscopy (Figure 4). In hydra exposed to 50 nm NPs, a significant increase in

208   polarization was observed at the highest concentration tested (80 mg/L). There was no significant

209   increase in polarization after the 24h depuration period. In hydra exposed to the 100 nm NPs, a

210   significant increase in polarization was found at concentrations > 2.5 mg/L. Increased polarization

211   persisted after the 24h depuration period at 5 mg/L.   Correlation analysis revealed that LCs

212   formation (polarisation) was significantly correlated with total lipids (r= 0.40) and NPs in tissues

213   (r=0.46) (Table 2). Changes in levels of polar lipids and LPO were also studied in hydra exposed

214   to the NPs (Figure 5A to 4D). In hydra exposed to 50 nm NPs, the levels of polar lipids were

215   significantly increased at concentrations between 5 and 80 mg/L (Figure 5A). The lipids levels

216   returned to control values after the 24h depuration period. The levels of LPO followed a biphasic

217   response where the levels were increased at low concentrations (1.25 to 5 mg/L) followed by a

218   decrease at higher concentrations where morphological effects were observed (Figure 5B). After

219   the 24h depuration period, LPO levels in controls were higher than the 96h control but the levels

220   returned to control values at 5 mg/L. In hydra exposed to the 100 nm NPs, the polar lipids levels

221   were significantly increased at concentrations $\geq$ 5 mg/L with the exception of the 40 mg/L owing

222   to data variability (Figure 5C). This effect persisted for the 5 mg/L treatment after the 24h

223   depuration period. Lipids levels were significantly correlated with viscosity (r=0.59) (Table 2).

224   LPO levels were significantly increased at concentrations $\geq$ 2.5 mg/L in respect to controls (Figure

225   5D). Oxidative stress persisted after the 24h depuration period with the 1.25 and 5 mg/L NP

226   concentration.

227   In the attempt to gain a global view on the effects of NPs on hydra, a principal component analysis

228   was performed on the 50 and 100 nm diameter NPs (Figure 6). In hydra exposed to the 50 nm NPs,

229   62 % of the total extracted variance was obtained with the biomarkers used in the present study

230   (Figure 6A). The most significant biomarkers were NPs levels in tissues (exposure), viscosity, LCs

231   and polar lipids (biomarkers of effects). Tissue levels of NP were closely related with lipids and

232   changes in viscosity. In hydra exposed to the more toxic 100 nm NPs, 60% of the total variance

233   was explained by the endpoints used in the study (Figure 6B), with NP, LCs formation, LPO and

234   viscosity changes being the most important biomarkers. NPs in tissues were closely related with

235   LPO, lipids levels and LC formation but weakly associated with viscosity. Lipids levels and the

236   formation of organized LCs where closely associated with each other which suggests that toxicity

237   involves the formation of organized (anisotropic) LCs in hydra exposed to NPs.

238   Discussion

239   The 100 nm diameter NP was 1.7 times more toxic than the 50 nm diameter NP on a particle

240   concentration basis. The EC50 for morphological changes was 3.6 and 18 mg/L for the 50 and 100

241   nm NPs respectively which was in the same range of the LC50 values (4.8 and 8.9 mg/L for 70

242 and 100 nm diameter NPs) for *Artemia salina* shrimp exposed to the polystyrene NPs in saline

243 waters (Mishra et al., 2019). In this study the smaller NPs showed more toxicity on a mass basis

244 than the larger ones as observed in *Hydra attenuata* but the equivalent amount of particles was not

245 provided. NPs produced oxidative stress as determined by LPO expression in hydra, which were

246 also induced in *Artemia,* corroborating our findings that polystyrene NPs produce oxidative

247 damage. Although oxidative stress (LPO) was involved in hydra exposed to the NPs, LPO levels

248 were more closely associated with levels of the 100 nm diameter NP than the 50 nm NP based on

249 principal component analysis. This could be explained by the observation of hydra losing their

250 tentacles at high concentrations of NPs potentially contributing to the variability in the levels of

251 internal NPs and oxidative stress. This is consistent with the peculiar bell-shaped response

252 obtained for LPO in hydra exposed to the 50 nm NPs. Oxidative stress was also observed in acs-

253 22 mutant *Caernorhabditis elegans* (nematodes) exposed to polystyrene NPs (Qu et al., 2018).

254 The NPs dysregulated some of the genes involved in the control of oxidative stress and activated

255 the expression of Nrf signaling which governs the antioxidant response pathway. In another study

256 with *C. elegans*, the uptake of 50 and 200 nm polystyrene NPs induced changes in metabolic

257 profiles and toxicity (Kim et al., 2019). The uptake of these NPs lead to perturbation in energy

258 metabolism (glucose and lactate) with induction of oxidative stress leading to reductions in

259 locomotion and reproduction. These observations are consistent with the present study were

260 reduction in tentacles and biomass were observed in hydra exposed to the NPs. In *Daphnia pulex*,

261 polystyrene NPs induced stress defence and immobilization during a 21-day exposure regime (Liu

262 et al., 2019). Indeed, as the fluorescent NP increased in the water fleas, genes involved in

263 antioxidant pathways (superoxide dismutase, catalase and glutathione S-transferase) initially

264 increased, followed by a decrease in gene expression. In zebrafish embryos, smaller-size

265 polystyrene NPs accumulated in lipid-rich regions such as in the egg yolk sac (Lee et al., 2019).

266 Oxidative stress and inflammation were also observed in zebrafish embryos exposed to the NPs.

267 This is consistent with the increase in polar lipids in hydra exposed to the NPs where the NPs in

268 tissues were significantly correlated with polar lipids, viscosity and the formation of organized

269 lipid-like LCs. This suggests that NPs could mobilize lipids into forming organized liquid crystal

270 and perhaps increasing oxidative damage in cells. The mobilization of lipids could also result from

271 the decreasing in hydra biomass (decrease in energy). For the 50 nm NPs, an analysis of covariance

272 of lipids levels with biomass as the covariate revealed that both the exposure concentration

273 (p=0.002) and biomass reduction (p=0.02) were significant, suggesting that both processes

274 occurred where the concentration of NPs was higher. In the case of 100 nm NPs, covariance

275 analysis revealed that the exposure concentration significantly influenced lipid levels with loss of

276 biomass having no significant effect. This suggests that lipids were mobilized in respect to NPs

277 exposure where a loss of biomass (fasting effect) had little influence on lipid contents in hydra.

278 The introduction of hydrophobic NPs such as polystyrene in cells could disrupt the conformational

279 changes of proteins and lipid organisation in the cytoplasm. For example in zebrafish embryos

280 exposed to NPs, the nanoparticles partitioned in lipid-rich environment of the yolk sac and induced

281 the expression of protein chaperones: heat shock proteins 70 and 90 (Kim et al., 2019).

282 Interestingly, the more toxic 100 nm NP revealed that NP in tissues were more closely associated

283 with organized lipid-like LCs and LPO in hydra. The FOE probe for LCs evaluation is composed

284 of an aliphatic carbon chain with a polar head (fluorescein) which can interact in hydrophobic

285 environments (lipid-like) which polarize fluorescence. Preliminary experiments revealed that NPs

286 alone do not significantly influence polarization but when combined with the post-mitochondrial

287 fraction, polarization occurs (Gagné et al., 2019a). It was proposed that fluorescence polarization

288   occurs at the lipid/protein corona of the NPs given the hydrophobic nature of the FOE probe.The

289   formation of lipid corona in addition to protein corona was also reported with other nanoparticles

290   such as colloidal gold (Zhang et al., 2018). Although the formation of lipid corona on gold

291   nanoparticles was governed by electrostatic interactions (cations at the surface proving better to

292   attract lipids than anionic charged nanoparticles), hydrophobic interactions could also induce

293   organized structures on the surface of polystyrene NPs (Gagné et al., 2019). In another study, oleic

294   acid-coated iron oxide nanoparticles were also toxic to neuronal cells (Fernandez-Bertolez et al.,

295   2018). Although the coated iron oxide nanoparticles were moderately toxic to cells, the compound

296   was able to produce single stranded DNA damage and reduced DNA repair activity in the presence

297   of H_2O_2 (oxidative stress). In human astrocytes, exposure to oleic acid-coated iron oxide

298   nanoparticles was also genotoxic, inducing primary DNA damage as determined by the comet

299   assay (Fernandez-Bertolez et al., 2019). However, the damage was seemingly reversible given that

300   no permanent cytogenetic damage (micronuclei) was observed. In conclusion, polystyrene NPs

301   were bioavailable to hydra and persisted after a 24 h depuration period. The 100 nm NPs was

302   more toxic than the 50 nm NP when compared on particle concentration basis. Toxicity was

303   dependent on the interaction between NP levels in hydra, lipids, the formation of organized LCs

304   and oxidative stress. The mobilization of lipids by the NPs could represent a mechanism for the

305   elimination of NPs from cells but could increase the toxicity (bioactivation) of NPs during this

306   process.

307

310   References

311   Al-Salem S, Lettieri P., Baeyens J. Recycling and recovery routes of plastic solid waste (PSW): a
312   review. Waste Manag. 29: 2625-2643, 2009.

313   Blaise, C., Kusui, T. Acute toxicity assessment of industrial effluents with a microplate-based
314   *Hydra attenuata* assay. Environ. Toxicol. Water Qual. 12: 53–60, 1997.

315   Bradford, M.M. A rapid and sensitive method for the quantitation of microgram quantities of
316   protein utilizing the principle of protein-dye binding. Anal. Biochem. 72: 248–254, 1976.

317   Colvin VL, Kulinowski KM, Nanoparticles as catalysts for protein fibrillation. PNAS 104:
318   8679–8680, 2007.
319
320   Fernández-Bertólez N, Costa C, Brandão F, Kiliç G, Teixeira JP, Pásaro E, Laffon BV.
321   Neurotoxicity assessment of oleic acid-coated iron oxide nanoparticles in SH-SY5Y cells.
322   Toxicology 406-407 : 81-91. 2018.

323   Fernández-Bertólez N, Costa C, Brandão F, Duarte JA, Teixeira JP, Pásaro E, Valdiglesias V,
324   Laffon B. Evaluation of cytotoxicity and genotoxicity induced by oleic acid-coated iron oxide
325   nanoparticles in human astrocytes. Environ Mol Mutagen. In press, 2019.

326   Finney DJ. Statistical Methods in Biological Assay, 2nd ed. Griffin, London, England, 1964.
327
328   Gagné F. Oxidative stress, Chap 6. In: Biochemical Ecotoxicology: Principle and Methods, New
329   York, Elsevier Inc. pp. 103-115, 2014.
330
331   Gagné F. Detection of polystyrene nanoplastics in biological tissues with a fluorescent molecular
332   rotor probe. J. Xenobiotics 9: 8147-8149, 2019.
333
334   Gagné F, Auclair J, André C. Polystyrene nanoparticles induce anisotropic effects in subcellular
335   fraction of the digestive system of freshwater mussels. Curr. Top. Toxicol. 15: 43-49, 2019a.
336
337   Gagné, F., Auclair, J., Quinn, B. Detection of polystryrene nanoplastics in biological samples
338   based on the solvatochromic properties of Nile Red: application in *Hydra attenuata* exposed to
339   nanoplastics. Environ. Sci. Poll. Res.: 2019b.

340   Greenspan P, Fowler SD. Spectrofluorometric studies of the lipid probe, Nile red. J Lipid Res. 26:
341   781-978, 1985.

342   Kim HM, Lee DK, Long NP, Kwon SW, Park JH. Uptake of nanopolystyrene particles induces
343   distinct metabolic profiles and toxic effects in *Caenorhabditis elegans*. Environ. Pollut. 246:
344   578-586, 2019.

345   Haidekker MA, LingT, Anglo M, Stevens HY, Frangos JA, Theodorakis EA. New fluorescent
346   probes for the measurement of cell membrane viscosity. Chemistry & Biology 8: 123-131, 2001.

347   Ho BT, Roberts TK, Lucas S. An overview on biodegradation of polystyrene and modified
348   polystyrene: the microbial approach. Crit. Rev. Biotechnol. 38: 308-320, , 2018.

349 Lambert S, Wagner M. Characterisation of nanoplastics during the degradation of polystyrene.
350 Chemosphere 145: 265-268, 2016.

351

352 Lee WS , Cho HJ , Kim E , Huh YH , Kim HJ , Kim B , Kang T , Lee JS , Jeong J .
353 Bioaccumulation of polystyrene nanoplastics and their effect on the toxicity of Au ions in
354 zebrafish embryos. Nanoscale 11: 3173-3185, 2019.

355

356 Liu Z, Yu P, Cai M, Wu D, Zhang M, Huang Y, Zhao Y. Polystyrene nanoplastic exposure
357 induces immobilization, reproduction, and stress defense in the freshwater cladoceran *Daphnia*
358 *pulex*. Chemosphere 215: 74-81, 2019.

359 Mishra P, Vinayagam S, Duraisamy K, Patil SR, Godbole J, Mohan A, Mukherjee A,
360 Chandrasekaran N. Distinctive impact of polystyrene nano-spherules as an emergent pollutant
361 toward the environment. Environ Sci Pollut Res Int. 26: 1537-1547, 2019.

362 Murphy, F., Quinn, B. The effects of microplastic on freshwater *Hydra attenuata* feeding,
363 morphology & reproduction. Environ. Poll. 234: 487-494, 2018.

364

365 Qu M, Xu K, Li Y, Wong G, Wang D. Using acs-22 mutant *Caenorhabditis elegans* to detect the
366 toxicity of nanopolystyrene particles. STOTEN 643: 119-126, 2018.

367 Pascoe D, Karntanut W, Müller CT. Do pharmaceuticals affect freshwater invertebrates? A study
368 with the cnidarian Hydra vulgaris. Chemosphere 51: 521-5238, 2003.

369

370 Quinn B, Gagné F, Blaise C. Hydra, a model system for environmental studies. Int. J. Dev. Biol.
371 56: 613-625, 2012.

372

373 Verschoor A, ban Herwijnen R, Postuma C, Klesse K., Werner S: Assessment document of land-
374 based inputs of microplastics in the marine environment. Environmental Impact of human
375 activities Series, OSPAR 2017; https://www.ospar.org/documents?v=38018

376 Wang F, Bexiga MG, Anguissola S, Boya P, Simpson JC, Salvati A, Dawson KA, Time resolved
377 study of cell death mechanisms induced by amine-modified polystyrene nanoparticles. Nanoscale
378 5: 10868-10876, 2013.

379

380 Wilby OK. The Hydra regeneration assay. In: Proceedings of the Workshop Organised by
381 Association Francaise de Teratologie. pp. 108–124, 1989.

382 Zhang X, Pandiakumar AK, Hamers RJ, Murphy CJ. Quantification of Lipid Corona Formation
383 on Colloidal Nanoparticles from Lipid Vesicles. Anal. Chem. 90: 14387-14394, 2018.

384

385

386
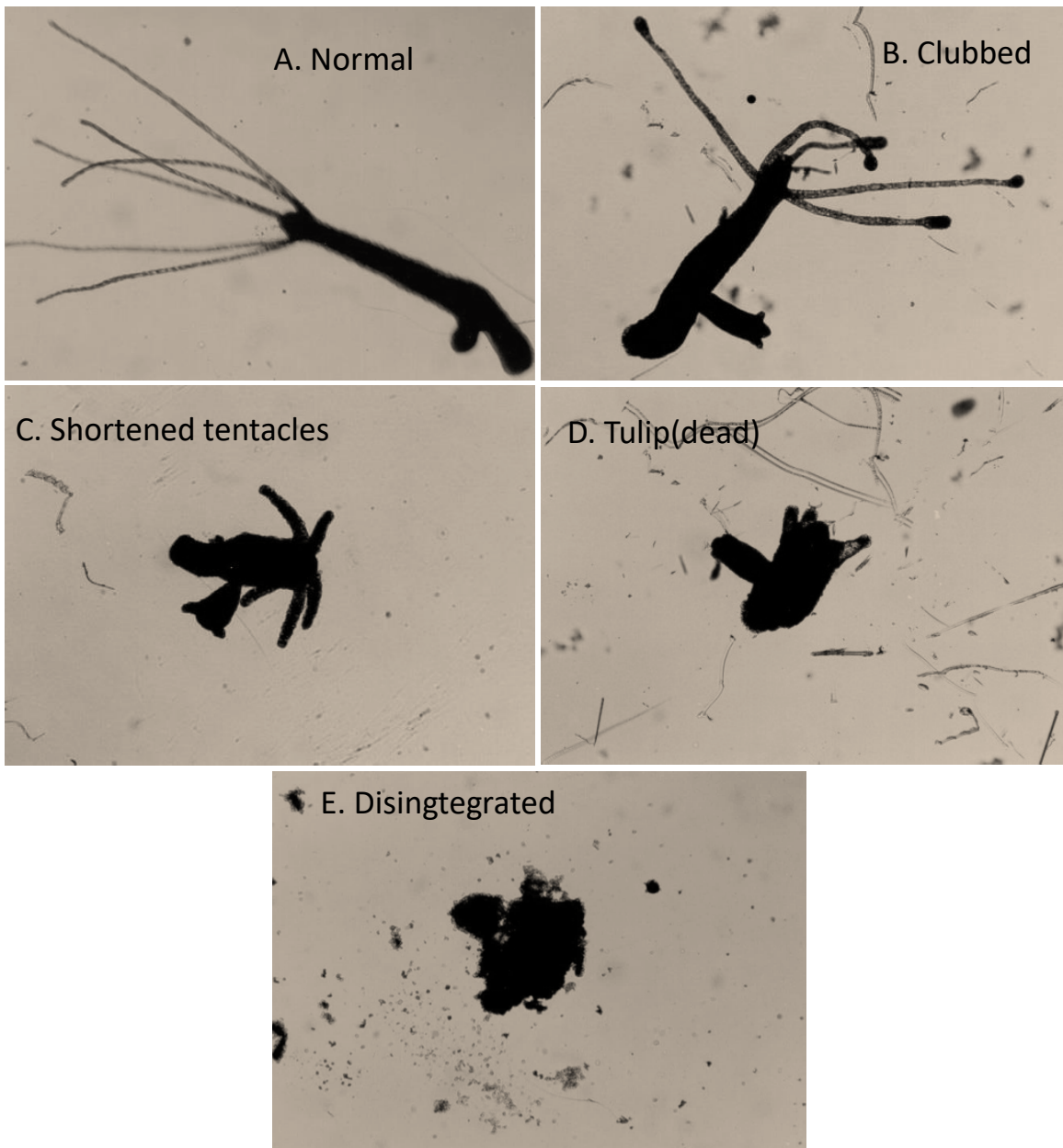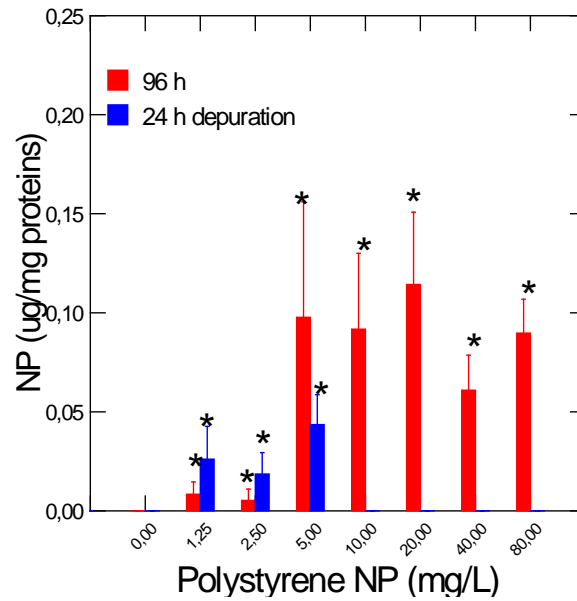
Figure 1. Morphological stages in *Hydra attenuate* after exposure to REEs for 96h (magnification x40): healthy polyp (A); clubbed tentacles (B); shortened tentacles(C); tulip stages (D) and disintegrated stage (E).
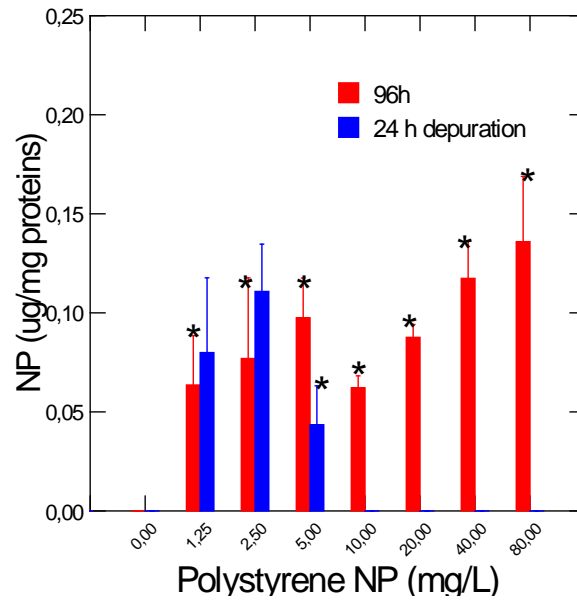
423

424   A 50 nm NP

425

426

427   B 100 nm NP

428

Figure 2. Detection of NP in *Hydra attenuata* using a molecular rotor probe.
Hydra were exposed to increasing concentrations of 50 nm (A) and 100 nm (B) polystyrene
nanoplastics for 96 h at 20°C. A subset of organisms were placed in clean media for 24 h for
depuration. The data represent the mean with the standard error. The star * symbol indicated
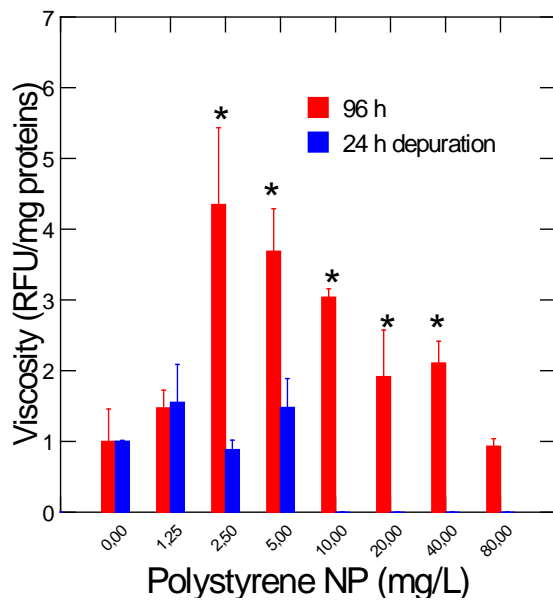significance from controls (0) at $p < 0.05$.

434

435
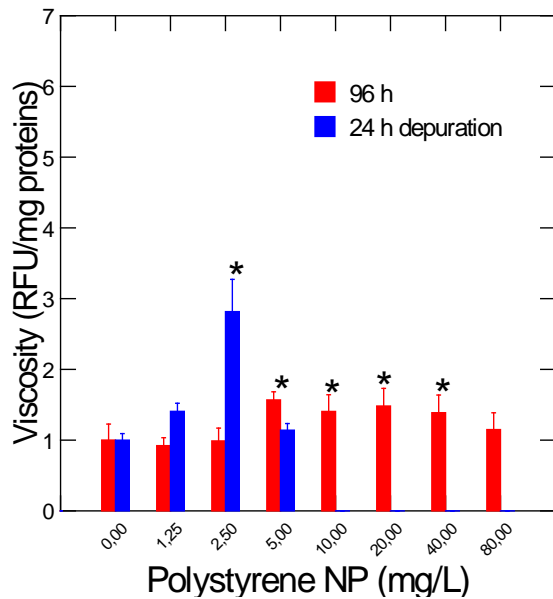
A 50 nm NPs

B 100 nm NPs
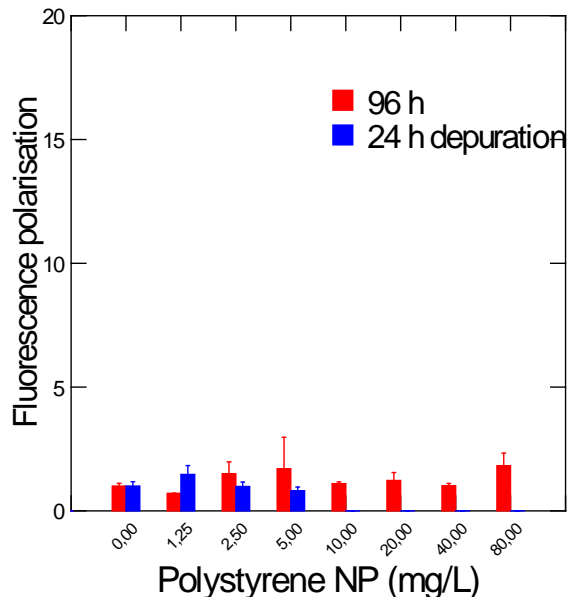

Figure 3. Change in viscosity in *Hydra attenuata* tissues exposed to NPs
Hydra were exposed to increasing concentrations of 50 nm (A) and 100 nm (B) polystyrene nanoplastics for 96 h at 20ºC. A subset of organisms were placed in clean media for 24 h for depuration. The data represent the mean with the standard error. The star * symbol indicated significance from controls at $p < 0.05$.
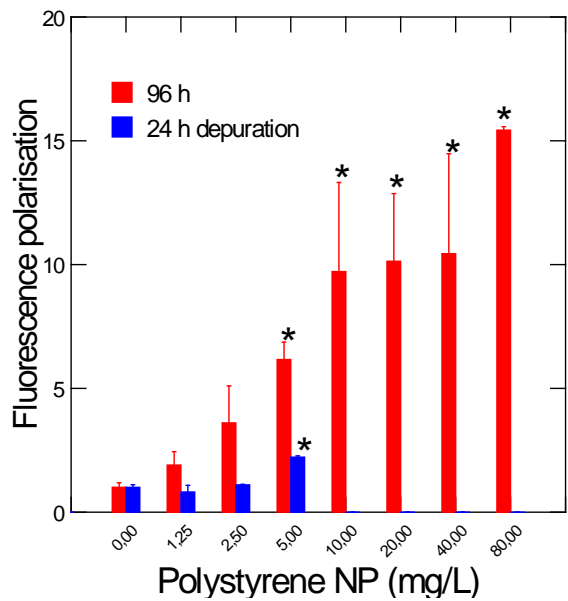
447 A 50 nm NPs

448

449 B 100 nm NPs

450

451 Figure 4. Formation of lipid-like liquid crystals in *Hydra attenuata* exposed to NPs.
452 Hydra were exposed to increasing concentrations of 50 nm (A) and 100 nm (B) polystyrene
453 nanoplastics for 96 h at 20ºC. A sub-set of organisms were placed in clean media for 24 h for
454 depuration. The data represent the mean with the standard error.The star * symbol indicated
455 significance from controls (0) at p<0.05.

456
457
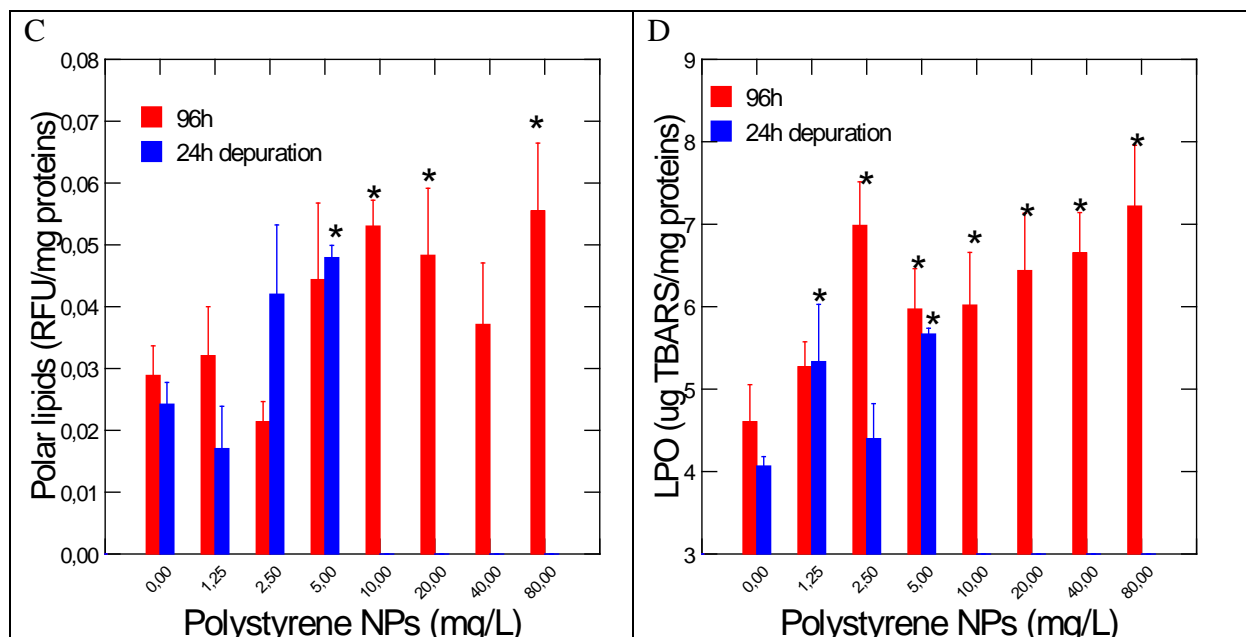

458

459   A 50 nm NPs

460

461   B 100 nm NPs
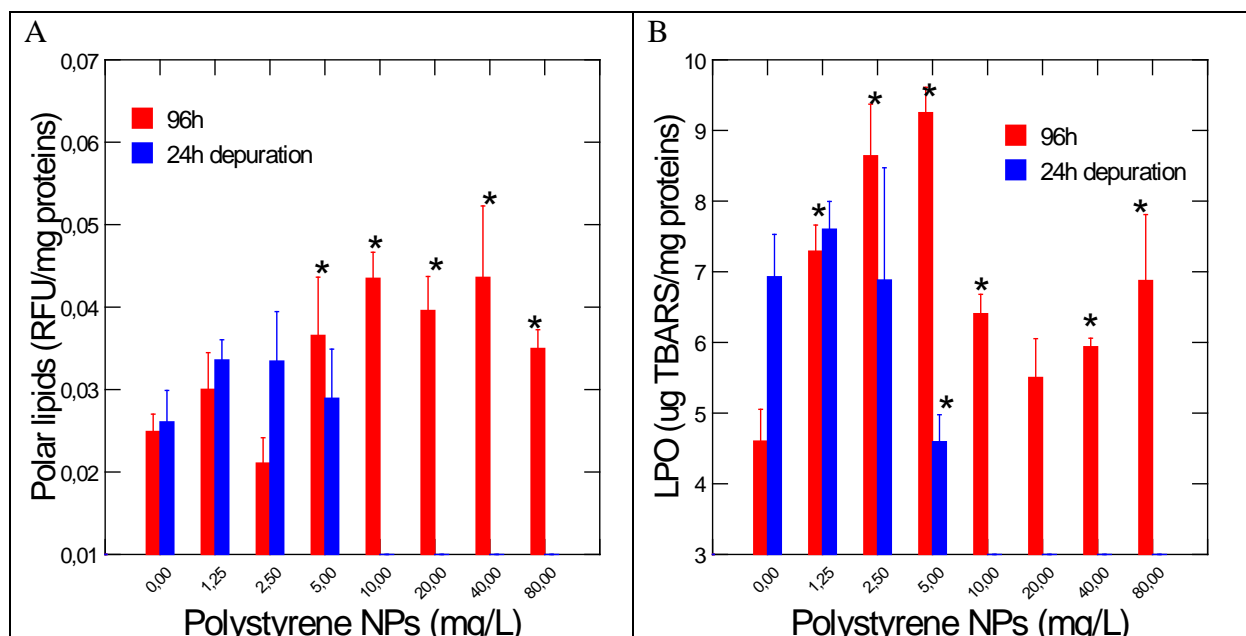
462

463   Figure 5. Changes in lipid contents and oxidative stress in *Hydra attenuata* exposed to NPs

464   Hydra were exposed to increasing concentrations of 50 nm (A) and 100 nm (B) polystyrene
465   nanoplastics for 96 h at 20ºC. A subset of organisms were placed in clean media for 24 h for
466   depuration. The data represent the mean with the standard error. The star * symbol indicated
467   significance from controls (0) at $p < 0.05$.
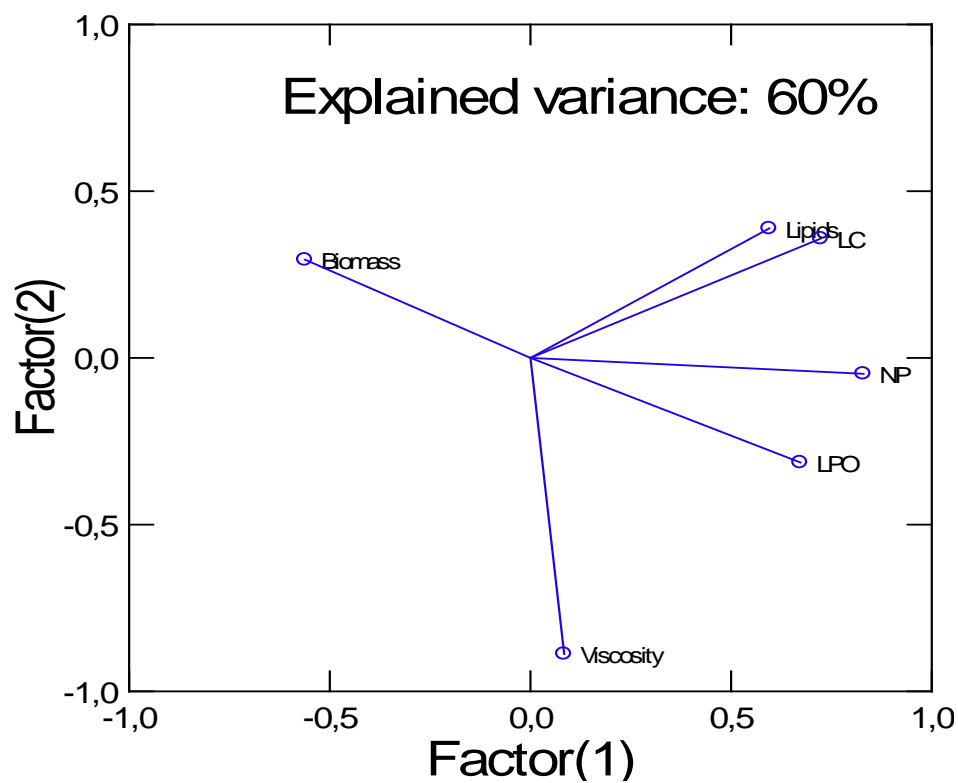
468

469 A 50 nm NPs
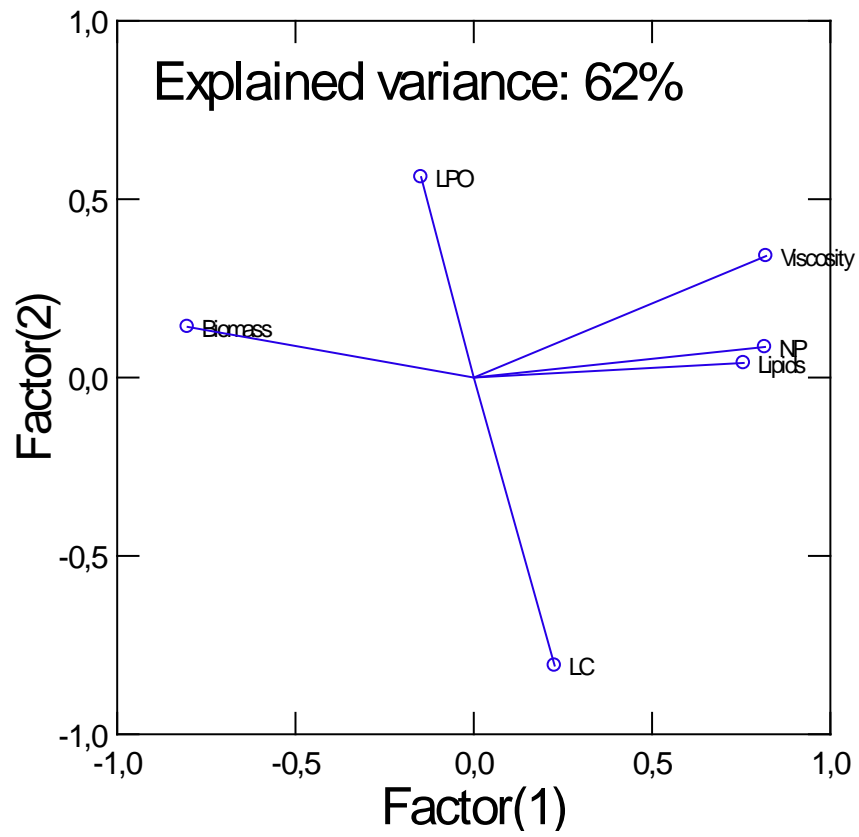
470

471

472 100 nm NPs

Figure 6. Factorial analysis of biomarker data in *Hydra attenuata* exposed to 50 nm (A) and 100 nm (B) NPs. The biomarker responses were analyzed using principal component analysis.

477

478 Table 1. Toxicity data of *Hydra attenuata* exposed to 50 and 100 nm polystyrene NPs

NP	LC50 in mg/L (95% confidence)	EC50 in mg/L (95% confidence)	Biomass[1] (EC50)	Observation
50 nm	> 80 mg/L	3.6 (3-4.7)	14 mg/L	White deposits on antennae at >5 mg/L
100 nm	> 80 mg/L	18.4 (14-25)	28 mg/L	White deposits on antennae at >5 mg/L

479 1. Concentration that decrease the turbidity at 600 nm of hydra homogenates by 50 %.

480

481

482

483 Table 2. Correlation analysis Table 1. Toxicity data of Hydra attenuata exposed to 50 and 100 nm
484 polystyrene NPs

485

486

487 50 nm NP

50 nm NP		Biomass	Lipids	NPs	Viscosity	LC	LPO
Biomass	¦	1					
Lipids	¦	**-0.38**	1				
NP	¦	**-0.59**	**0.49**	1			
Viscosity	¦	**-0.56**	**0.59**	**0.60**	1		
LC	¦	-0.31	0.09	0.09	-0.04	1	
LPO	¦	0.03	-0.20	-0.08	0.03	-0.08	1

100 nm NP		Biomass	Lipids	NPs	Viscosity	LC	LPO
Biomass	¦	1					
Lipids	¦	-0.18	1				
NP	¦	**-0.44**	0.33	1			
Viscosity	¦	-0.18	-0.10	0.02	1		
LC	¦	-0.23	**0.40**	**0.46**	-0.15	1	
LPO	¦	-0.15	0.21	**0.50**	0.25	**0.35**	1

507 Significant correlations (p<0.05) are highlighted in **bold.** NP: Nanoplastics in hydra, LC: liquid
508 crystals (fluorescence polarisation), LPO: lipid peroxidation.